Multiple directional enhanced light source through a periodic metal grating structure

**Le Yu (余 乐)[1,2], Xiao Xiong (熊 霄)[1,2], Di Liu (刘 頔)[1,2], Lantian Feng (冯兰天)[1,2],
Ming Li (李 明)[1,2], Linjun Wang (汪林俊)[3], Guoping Guo (郭国平)[1,2],
Guangcan Guo (郭光灿)[1,2], and Xifeng Ren (任希锋)[1,2,*]**

[1]*Key Laboratory of Quantum Information, CAS, University of Science and Technology of China,
Hefei, 230026, China*

[2]*Synergetic Innovation Center of Quantum Information & Quantum Physics, University of Science and
Technology of China, Hefei, 230026, China*

[3]*Center for Micro- and Nanoscale Research and Fabrication, University of Science and Technology of China,
Hefei, 230026, China*

*Corresponding author: renxf@ustc.edu.cn

Received February 11, 2017; accepted April 28, 2017; posted online May 27, 2017

Higher emission rates and controllable emission direction are big concerns when it comes to finding a good single photon source. Recently, surface plasmons are introduced to this application, as they can manipulate and enhance the luminescence of single emitters. Here, we experimentally achieve a wide-area multiple directional enhanced light source through periodic metal grating structures. The surface-plasmon-coupled emission can have multiple precisely emission angles by just changing the period of the grating. Our result indicates that metal plasmonic grating can be used as a productive quantum device for unidirectional quantum light sources in quantum optics.

OCIS codes: 240.6680, 070.0070, 050.0050.
doi: 10.3788/COL201715.082401.

In recent years, semiconductor quantum dots (QDs) have been widely used as photon sources in quantum optics due to their special properties[1–4], such as high quantum efficiency[5], narrow and tunable emission spectrum[6], easy manipulation[7], and so on. The spontaneous emission of QDs also depends on the surrounding environment[8]. For example, people put QDs in a cavity to enhance their emissions, which is known as the Purcell effect[9]. Additionally, surface plasmon polaritons (SPPs) are also used to enhance the luminescence intensity[10–13], which are collective charge oscillations on the surfaces of metals. SPPs could confine the electric field to the deep sub-wavelength scale and increase the density of the state of optical modes, thus increasing the spontaneous emission rates of QDs[14,15].

On the other hand, when putting QDs near periodic structures (such as photonic crystals, gratings, and so on), the QD emissions could be further modulated[16–24]. For instance, using photonic crystals, both the polarization and the propagation direction of the emissions could be engineered[25]. In particular, if the periodic structure is metallic, both propagated SPPs and localized SPPs are formed; thus, luminescence enhancement and emission modulation could be realized simultaneously[26–31].

It should be noted that the radiation of QDs near a smooth metal surface exhibits as a damped oscillator depending on the separation between QDs and metal[32]. If QDs are too close to the metal, most emissions will be dissipated through non-radiative paths, which is also known as the quenching effect[33]. Therefore, QDs usually need a thin layer of oxide coating to avoid quenching[34].

In this Letter, we utilized a plasmonic grating to demonstrate that the emission direction of the QDs' luminescence could be engineered by tuning the grating constants. In the meantime, the luminescence of QDs is also improved two times due to localized SPPs. This work may be useful for the investigation of quantum single-photon sources.

The experimental setup is shown in Fig. 1(a). For photoluminescence (PL) measurements, a continuous-wave laser at 532 nm was focused on the sample with an objective lens (OLYMPUS 100x, NA = 0.9). Then, the light emitted from the sample was collected with the same objective and sent to a spectrograph (Princeton Instrument Acton SP2500) after a dichroic mirror (DM). Two conjugate lenses and a pinhole are used to filter the background noise in a non-focal plane and non-focal points in the focal plane. In spite of the emission spectrum, we also studied the emission directionality with back focal plane imaging[35], which could transform the angle information into position information in the Fourier plane. An electron-multiply charge-coupled device (EMCCD) was put behind a series of lenses so that the fluorescence in the back focal plane was collected. Through the positions of the lights in the back focal plane, we obtain the emission direction of the PL from the grating intuitively.

We use the electron beam evaporation coating technique to coat a 140-nm-thick Au film on a silica substrate (with 10-nm-thick Ti as an adhesive). Then, we use focused ion beam (FIB, FEI Company Helios 650) lithography to pattern an Au grating onto an SiO₂ substrate.
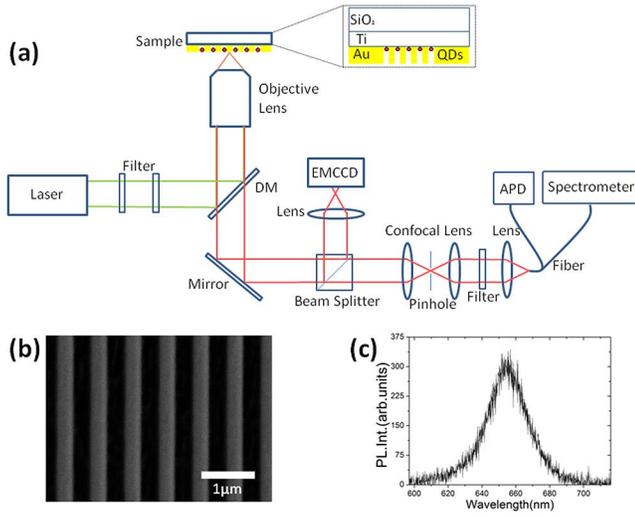
(a)

(b)

Fig. 1. (a) Schematic description of the experimental setup. (b) The SEM image of the metal grating sample; the period of the grating is about 450 nm. (c) Luminescence spectrum of QDs.
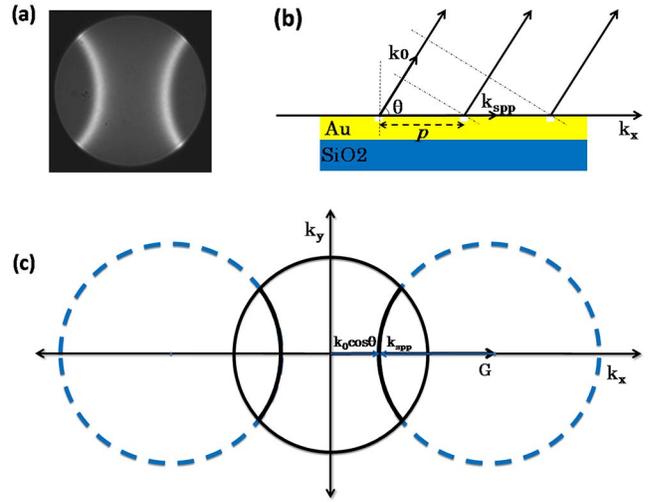

Fig. 2. (Color online) (a) The back focal plane image of the luminescence in grating sample A. (b) Phase relation for wave vectors of emissions and SPPs. k_0 represent the actual direction of the emission light, and p is the grating period. (c) Schematic image of the Fourier plane. The black circle represents the actual view field, which we can observe from the back focal plane.

The FIB milling parameter is 30 kV accelerated voltage and a 24 pA ion current. The milling time is controlled to get Au gratings etched through (transparent Au grating) and not (opaque Au grating). We made five samples, called samples A (grating sample $p = 450$ nm), B ($p = 500$ nm), C ($p = 650$ nm), D ($p = 850$ nm), and E ($p = 1050$ nm). Last, we use atomic layer deposition (ALD) to deposit 10 nm Al_2O_3 as the isolation layer to avoid the direct contact of the QDs and the Au film (avoiding the quenching effect). It has been shown that the optimal spacing between the QDs and metal is about 11 nm[36]. The QDs were dispersed onto the Au grating by spin coating and were diluted from the QDs solution in decane. We also did experiments for the control group, in which QDs are deposited onto a bare silica substrate.

Figure 1(b) displays the scanning electron microscope (SEM) image of our grating sample A, with a grating period of 450 nm. The QDs we used were colloidal CdSe core/ZnS shell QDs. The PL spectrum of a typical QD with a 4-nm-diameter-core and a few nanometers shell is shown in Fig. 1(c) and peaked at 655 nm. The initial quantum yield of the QDs is about 0.5.

Figure 2(a) displays the back focal plane image of the QDs emissions for sample A, which have two arcs inside a circular view field. The circular view field represents the collection area of our objective, which is determined by the NA of the objective lens. The gray background inside the view field comes from the free emission of the QDs, since we collected the reflected signal. The two bright arcs correspond to the SPP-coupled emission (SPCE). For a typical SPCE (the emission of QDs deposited on a metal film), we expect the back focal plane image to be a ring, since luminescence is emitted at a specific angle according to the momentum matching condition. The reason for obtaining two arcs in our experiment is that the grating modified the QDs' emission direction.

A quantitative explanation is as follows. Because the wave vector of the SPPs is larger than that of the PL at the same frequency, the SPCE will not happen during propagation on a flat surface since the momentum does not match. When a grating with period p is introduced, the SPPs are scattered into free space at each tooth and interfere with each other. As shown in Fig. 2(b), the phases of SPCE between adjacent teeth should satisfy (in the X-direction on the X–Z plane):

$$k_0 p \cos \theta - k_{\mathrm{spp}} p = \pm n \cdot 2\pi. \tag{1}$$

Divided by p on both sides, we get

$$k_0 \cos \theta = k_{\mathrm{spp}} \pm nG = \sqrt{\frac{\varepsilon_{\mathrm{air}} \varepsilon_{\mathrm{Au}}}{\varepsilon_{\mathrm{air}} + \varepsilon_{\mathrm{Au}}}} k_0 \pm nG. \tag{2}$$

Here, k_0 is the wave vector of the emitted light in free space, k_x is the axis whose direction is perpendicular to the direction of the grating groove inside the sample plane, k_y is vertical to k_x, θ is the angle between k_x and k_0, k_{spp} is the wave vector of the surface plasmon propagating in the metal grating, $\varepsilon_{\mathrm{air}}$ and $\varepsilon_{\mathrm{Au}}$ are the permittivity of air and gold. $G = 2\pi/p$ is the grating vector, and n is an integer.

The schematic momentum diagram of Eq. (2) is shown in Fig. 2(c). The solid black circle represents the view field of our objective, whose radius is NA^*k_0 (NA = 0.9 in our experiment). The two dotted blue circles correspond to the propagating SPPs. They are shifted by $\pm G$ (toward the left and right for $n = \pm 1$, respectively) due to the Au grating, resulting in two arcs inside the view field that can be observed with back focal plane imaging. With different G, the SPCE can be tuned to different emission directions.

Note that the dotted blue circles are shifted along the k_x-axis only here because our grating is 1D. That is the reason why we observe the arcs' shapes. If the grating is 2D, we then can engineer the SPCE to be shifted along the whole k-plane, and the emission of QDs can be fully controlled into arbitrary direction.

The experimental results are displayed in Fig. 3. We measured five samples, which are labeled as samples A, B, C, D, and E, with different grating constants 450, 500, 650, 850, and 1050 nm [Figs. 3(a)–3(e)]. The corresponding back focal plane images are shown as Figs. 3(f)–3(j), respectively. We noticed that the image patterns are not the same, which can be explained as follows. According to Eq. (2), when p is small, G is so large that only the first-order ($n = 1$) SPCE can be collected by our objective [see Figs. 3(f)–3(h)]. As p increases, G decreases; thus, the high-order SPCE also emerges inside the view field [see Figs. 3(i)–3(j)]. The accurate emission angles for the different-order SPCEs of the five samples are summarized in Table 1, shown below.

Note that, for sample C, $k_{\text{spp}} \approx G$, resulting in $\theta \to 90°$ when $n = 1$. So the two arcs are very close to each other, as shown in Fig. 3(h). In fact, it also has a second-order SPCE with $\theta = 14.8635°$, but this is not visible in Fig. 3(h), because the emission angle exceeds the objective collection angle [$\arccos(\text{NA}) \approx 25.8°$]. With higher NA or using an oil immersion objective lens, more emissions could be observed. The fact that the signal-to-noise ratio (SNR) of our back focal images decreases as the grating constant increases is probably due to the energy dissipation to more channels (more radiation angles). We have also investigated the opaque samples that are not etched through (50-nm-thick Au grating on top of 150-nm-thick Au film). The results are presented in Figs. 3(k)–3(o). Obviously, the basic SPCE patterns with arcs remain the same, but the SNRs drop significantly compared to

Table 1. Directional Emission Angles for the Five Samples

Sample	θ		
	$n = 1$	$n = 2$	$n = 3$
A(450 nm)	66.0016°		
B(500 nm)	74.8614°		
C(650 nm)	87.6415°	14.8635°	
D(850 nm)	73.8438°	60.5061°	
E(1050 nm)	64.8471°	78.5347°	34.6557°

transparent samples. One possible reason is that more SPPs propagate along the Au film and dissipate, rather than being coupled to free space (the signal is decreased). Another reason is that probably the channel for the scattered SPPs to transmit to the silica substrate is forbidden (the noise is increased).

As we have analyzed, the propagating SPPs contribute to engineering the SPCE directionality via the grating. There are also localized SPPs in the Au grating, which would greatly enhance the luminescence of the QDs. The mechanism is the Purcell effect, which could be verified by measuring the emitter's spontaneous emission rate. As shown in Fig. 4, the lifetimes for the QDs on the bare silica substrate and Au grating are both measured. By fitting them with exponential functions, the lifetime of the QDs on the bare silica substrate is about 11 ns, while the lifetime of the QDs on the Au grating is about 3.3 ns, indicating a three times enhancement. We get a nearly two times enhancement in the experiment. We may have lost part because some energy was reduced in the propagating process in form of SPPs[37]. The experimental results are consistent with the previous Letter[38].
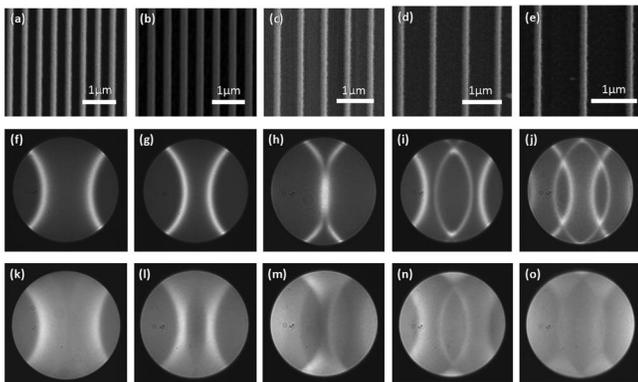
Fig. 3. (a)–(e) The SEM images of five samples, in which the Au gratings are etched through. The grating constants are (a) 450, (b) 500, (c) 650, (d) 850, and (e) 1050 nm, respectively. (f)–(j) The back focal plane images of the luminescence for the corresponding grating samples. (k)–(o) The back focal plane images of the luminescence for the corresponding grating samples, which have the same grating constant but are not etched through.
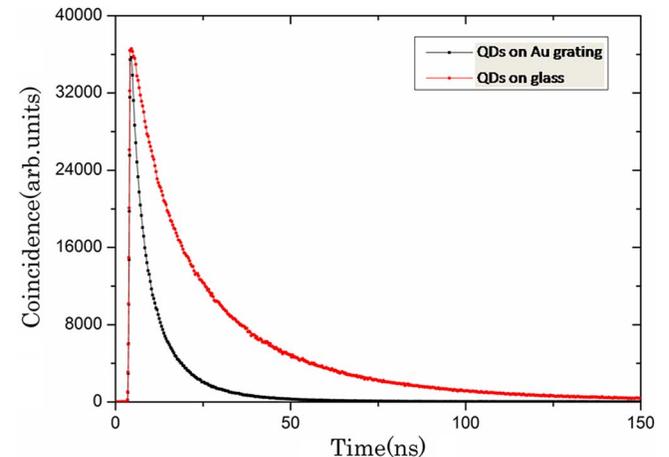
Fig. 4. (Color online) (a) The lifetime of QDs on bare silica substrate, where $t = 11.66$ ns. (b) The lifetime of QDs on the Au grating, where $t = 3.28$ ns.

In conclusion, we report an enhanced QDs photon source with directional emission using a plasmonic grating. The emission direction depends on the grating constant and the wavelength of QDs' luminescence. The emission intensity also gets enhanced by the localized SPPs in the grating, which is confirmed by the decrease of the QDs' lifetime. We also verify that a grating that is etched through is important in improving the SNR of the source. This grating-assisted directional photon source can be integrated on an optical chip and has great potential for developing an integrated directional single-photon source.

References

1. V. I. Klimov, A. A. Mikhailovsky, D. W. McBranch, C. A. Leatherdale, and M. G. Bawendi, Science **287**, 1011 (2000).
2. C. Murray, D. Norris, and M. Bawendi, J. Am. Chem. Soc. **115**, 8706 (1993).
3. K. T. Shimizu, W. K. Woo, B. R. Fisher, H. J. Eisler, and M. G. Bawendi, Phys. Rev. Lett. **89**, 117401 (2002).
4. L.-L. Wang, C.-L. Zou, X.-F. Ren, A.-P. Liu, L. Lv, Y.-J. Cai, F.-W. Sun, G.-C. Guo, and G.-P. Guo, Appl. Phys. Lett. **99**, 061103 (2011).
5. O. E. Semonin, J. M. Luther, S. Choi, H.-Y. Chen, J. Gao, A. J. Nozik, and M. C. Beard, Science **334**, 1530 (2011).
6. P. O. Anikeeva, J. E. Halpert, M. G. Bawendi, and V. Bulovic, Nano Lett. **9**, 2532 (2009).
7. J. N. Farahani, D. W. Pohl, H.-J. Eisler, and B. Hecht, Phys. Rev. Lett. **95**, 017402 (2005).
8. P. Lodahl, A. F. van Driel, I. S. Nikolaev, A. Irman, K. Overgaag, D. Vanmaekelbergh, and W. L. Vos, Nature **430**, 654 (2004).
9. E. M. Purcell, Phys. Rev. **69**, 37 (1946).
10. J. B. Khurgin, G. Sun, and R. A. Soref, J. Am. Opt. Soc. B. **24**, 1968 (2007).
11. D. Y. Lei and H. C. Ong, Appl. Phys. Lett. **91**, 211107 (2007).
12. K. Okamoto, I. Niki, A. Shvartser, Y. Narukawa, T. Mukai, and A. Scherer, Nat. Mater. **3**, 601 (2004).
13. V. J. Sorger and X. Zhang, Science **333**, 709 (2011).
14. J.-H. Song, T. Atay, S. Shi, H. Urabe, and A. V. Nurmikko, Nano Lett. **5**, 1557 (2005).
15. Z.-K. Zhou, D. Y. Lei, J. Liu, X. Liu, J. Xue, Q. Zhu, H. Chen, T. Liu, Y. Li, H. Zhang, and X. Wang, Adv. Opt. Mat. **2**, 56 (2014).
16. I. L. Medintz, S. A. Trammell, H. Mattoussi, and J. M. Mauro, J. Am. Chem. Soc. **126**, 30 (2004).
17. J. Zhang, J. Yang, H. Lu, W. Wu, J. Huang, and S. Chang, Chin. Opt. Lett. **13**, 091301 (2015).
18. B. Alén, F. Bickel, K. Karrai, R. J. Warburton, and P. M. Petroff, Appl. Phys. Lett. **11**, 83 (2003).
19. P. Frantsuzov, M. Kuno, B. Jankó, and R. A. Marcus, Nat. Phys. **4**, 519 (2008).
20. T. Ma, X. Yuan, W. Ye, W. Xu, S. Qin, and Z. Zhu, Chin. Opt. Lett. **12**, 020501 (2014).
21. T. Sadi, J. Oksanen, J. Tulkki, P. Mattila, and J. Bellessa, IEEE J. Sel. Top. Quantum Electron. **19**, 1 (2013).
22. T. Sadi, J. Oksanen, and J. Tulkki, IEEE J. Quantum Electron. **50**, 141 (2014).
23. R. Zhang, Y. Wang, Y. Zhang, Z. Feng, F. Qi, L. Liu, and W. Zheng, Chin. Opt. Lett. **12**, 020502 (2014).
24. B. Gallinet, A. M. Kern, and O. J. F. Martin, J. Opt. Soc. Am. A **27**, 2261 (2010).
25. P. Lodahl, A. F. van Driel, I. S. Nikolaev, A. Irman, K. Overgaag, D. Vanmaekelbergh, and W. L. Vos, Nature **430**, 654 (2004).
26. A. A. Darweesh, S. J. Bauman, and J. B. Herzog, Photon. Res. **4**, 173 (2016).
27. M. Li, C.-L. Zou, X.-F. Ren, X. Xiong, Y.-J. Cai, G.-P. Guo, L.-M. Tong, and G.-C. Guo, Nano Lett. **15**, 2380 (2015).
28. H. K. Fu, C. W. Chen, C. H. Wang, T. T. Chen, and Y. F. Chen, Opt. Express **16**, 6361 (2008).
29. E. Homeyer, P. Mattila, J. Oksanen, T. Sadi, H. Nykanen, S. Suihkonen, C. Symonds, J. Tulkki, F. Tuomisto, M. Sopanen, and J. Bellessa, Appl. Phys. Lett. **102**, 081110 (2013).
30. A. Kumar, J.-C. Weeber, A. Bouhelier, F. Eloi, S. Buil, X. Quélin, M. Nasilowski, B. Dubertret, J.-P. Hermier, and G. C. des Francs, Sci. Rep. **5**, 16796 (2015).
31. L. Lu, L.-L. Wang, C.-L. Zou, X.-F. Ren, C.-H. Dong, F.-W. Sun, S.-H. Yu, and G.-C. Guo, J. Phys. Chem. C **116**, 23779 (2012).
32. T. Pons, I. L. Medintz, K. E. Sapsford, S. Higashiya, A. F. Grimes, D. S. English, and H. Mattoussi, Nano Lett. **7**, 3157 (2007).
33. D. Englund, D. Fattal, E. Waks, G. Solomon, B. Zhang, T. Nakaoka, Y. Arakawa, Y. Yamamoto, and J. Vuckovic, Phys. Rev. Lett. **95**, 013904 (2005).
34. O. Kulakovich, N. Strekal, A. Yaroshevich, S. Maskevich, S. Gaponenko, I. Nabiev, U. Woggon, and M. Artemyev, Nano Lett. **2**, 1449 (2002).
35. A. G. Curto, G. Volpe, T. H. Taminiau, M. P. Kreuzer, R. Quidant, and N. F. van Hulst, Science **329**, 930 (2010).
36. T. Sadi, J. Oksanen, and J. Tulkki, J. Appl. Phys. **114**, 223104 (2013).
37. G. M. Akselrod, C. Argyropoulos, T. B. Hoang, C. Ciracì, C. Fang, J. Huang, D. R. Smith, and M. H. Mikkelsen, Nat. Photon. **8**, 835 (2014).
38. J. Zhang, Y.-H. Ye, X. Wang, P. Rochon, and M. Xiao, Phys. Rev. B. **72**, 201306 (2005).